

Joint interpretation of high-resolution velocity and resistivity models from the Barents Sea

Allan McKay^{1*}, Grunde Rønholt¹, Tashi Tshering¹ and Sören Naumann¹ demonstrate how they have used CSEM to determine background velocity and resistivity trends, and identify regions of anomalously high resistivity.

To realize the full potential of a geophysical data set, and resolve interpretation ambiguities, the data must be integrated with other geological and complementary geophysical data. Seismic velocity and electrical resistivity are rock properties that both depend on lithology and fluid content: we show that valuable insight can be gained by integrated interpretation of high-resolution velocity and resistivity models produced by inversion and imaging of broadband dual-sensor (GeoStreamer) and Towed Streamer EM data respectively.

Broadband dual-sensor seismic data enables high-resolution velocity model building and depth imaging using reflections, refractions and sea-surface multiples. As a result of advances in algorithms, workflows and high performance computing it is fast becoming routine to produce high resolution and accurate velocity models for large-scale 3D broadband dual-sensor data-sets as part of the depth imaging workflow. Thus seismic velocity is a rock property that can now be determined with sufficient resolution and precision to be of use to an interpreter in an exploration setting, before more detailed quantitative interpretation studies are undertaken.

Marine Controlled Source EM (CSEM) data has been used extensively to improve the chance of success in the search for hydrocarbons given that accumulations of oil and gas can be characterized by increased resistivity. CSEM data have been used mostly to de-risk prospects. By using a Towed Streamer EM system it is possible to acquire CSEM data efficiently to determine the sub-surface resistivity reliably at both regional and prospect scales.

Over the course of the past two years about 10,000 km² of co-incident 3D broadband dual-sensor and Towed Streamer EM data have been acquired in the Norwegian sector of the Barents Sea. Thus, there is a unique opportunity to integrate the high-resolution velocity and resistivity models provided by the broadband dual sensor and Towed Streamer EM data respectively. Previously published studies that have sought to exploit the relationship between seismic velocity and resistivity have generally used lower resolution stacking and/or migration velocity fields (e.g. Brevik et al., 2009; Werthmüller et al., 2013).

We are particularly interested in two aspects of the velocity-resistivity relationship. First of all, to cross-validate and appraise the recovered resistivity model by comparison against an independent rock property. Therefore, in the first instance we are interested primarily in examining the background trend in velocity and resistivity. Second, recognising the complimentary sensitivity of acoustic and electromagnetic data to changes in lithology and fluid then we illustrate how the resistivity model may help to provide support for and/or de-risk seismically driven prospects defined by a combination of structure (e.g. well defined closure) and other potential fluid indicators such as flat-spots and amplitude anomalies.

The structure of this paper is as follows. First, we introduce the motivation for this work in terms of examining the relationship between seismic velocity and resistivity in a clastic setting with a shale overburden, and sandstone reservoir. Second, we outline the data we have used and key aspects of the inversion and imaging methodology. Third, we highlight the main results where we focus on two aspects: verifying and determining the background velocity and resistivity trend, and identifying regions of anomalously high resistivity.

Motivation and interpretation framework

Seismic and electromagnetic data have complementary sensitivity to changes in rock fluid and lithology. The complementary sensitivity can be exploited by combining acoustic and electromagnetic parameters as part of the interpretation workflow. For example, MacGregor (2012) illustrated that by combining seismic and EM data it is possible to discriminate between three possible scenarios within a North Sea chalk prospect: tight (low porosity), water wet, and hydrocarbon charged. Only the hydrocarbon-charged scenario resulted in a combination of relatively low acoustic impedance (in comparison to tight chalk) and high resistivity. This kind of idea is summarized in Figure 1 for some other common lithology types.

Cross-property relations developed by Carcione et al. (2007) show that seismic velocity and resistivity trends are different for shales saturated with brine (e.g. the overburden), and sands saturated with oil (e.g. reservoir sands). As the velocity of a shale increases, then so does the resistivity:

¹PGS Geophysical AS.

* Corresponding author, E-mail: allan.mckay@pgs.com

EM & Potential Methods

The so-called Faust equation (Faust, 1953) provides an illustrative example of the relationship between bulk resistivity and seismic velocity (although as an empirical relation it has limited predictive power), viz.

$$\rho = \frac{\rho_f}{z} \left(\frac{v}{2.289} \right)^6 \quad (1)$$

Where ρ = bulk resistivity [ohm m], ρ_f = brine resistivity [ohm m], z is the depth [km], and v is velocity [km/s]. One obvious implication of the Faust equation is that the relationship between velocity and resistivity is non-linear.

In hydrocarbon saturated sands, however, the opposite behaviour is observed to that of shale: As the velocity of the sand increases, the resistivity decreases. When hydrocarbons replace brine in a sandstone rock then the seismic velocity decreases, but by only by a few per cent, but resistivity can increase by more than a factor of ten; see Figure 2 for example.

Data sets

Both data-sets cover the same area (about 10,000 km²) of the former disputed zone between Norway and Russia in the so-called Barents Sea South East (BSSE). The northern extent of the survey extends on to the Bjarmeland Platform; the southern extent encompasses the Veslekari Dome; see Figure 3.

The broadband dual-sensor seismic data were acquired using 12 streamers, 7 km long, 75 m apart and towed at a depth of 25 m. The relatively small streamer separation (compared to the more common 100 m for exploration surveys) was intended to improve illumination of shallow targets as one of the main plays (the Jurassic Sands of the Realgrunnen sub-group) in the BSSE is particularly shallow.

The Towed Streamer EM system enables large areas to be covered efficiently: With a typical sail-line spacing of

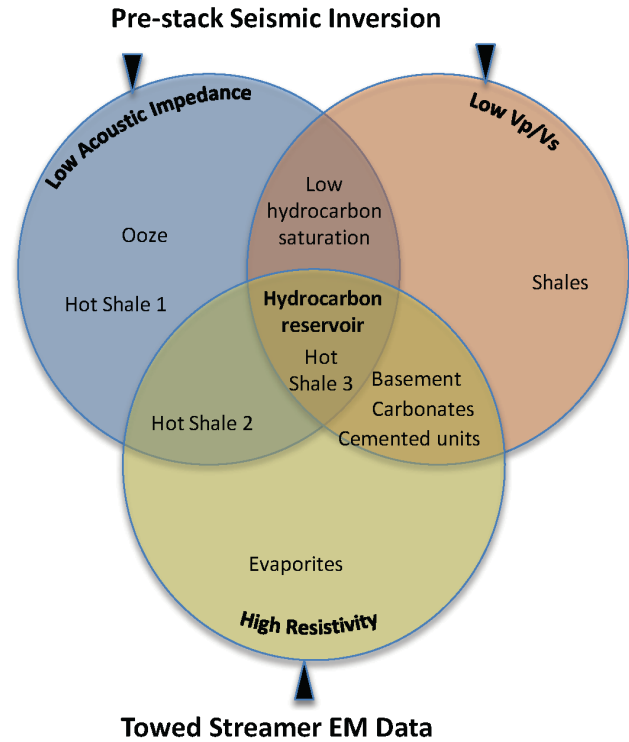


Figure 1 The power of integrated analysis by the reduction of solution ambiguity. Modified after Veggeland et al. (2014).

1 km then 3000 km² can be covered in about one-month. The system comprises a surface towed Horizontal Electric Dipole source and an EM streamer 8.7 km long, with 72 electric field channels. The source and streamer are towed at 10 m and 100 m depth respectively. See McKay et al. (2015), and references therein, for a complete description of the acquisition system.

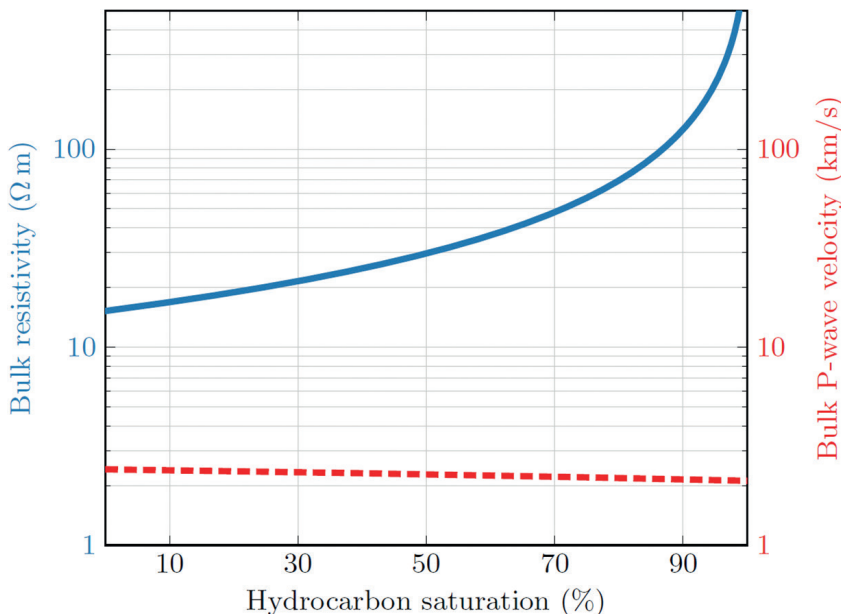


Figure 2 Seismic P-wave velocity and resistivity as a function of hydrocarbon saturation. After Werthmüller (2013), with the rock properties based on Table 1 of Carcione et al. (2007).

Acoustic and electromagnetic inversion and imaging methods.

Complete Wavefield Imaging Methodology

Acquiring 3D towed streamer seismic data in shallow waters always involves a compromise between efficiency and near-surface sampling. However, dual-sensor seismic data provides access to several components of the seismic wavefield: By utilizing all components of the wavefield in seismic imaging, including the up- and down-going wavefields, the angle illumination of the near surface can be improved significantly. Therefore, the 3D broadband dual-sensor seismic data was processed using a complete wavefield imaging workflow that, in addition to wavelet shift tomography and full waveform inversion (FWI), uses separated wavefield imaging (SWIM) to produce images and gathers that span the complete range of incidence angles. In addition to producing a high-resolution velocity model, Amplitude Versus Angle (AVA) analysis is enabled even for the relatively shallow plays of interest in the BSSE. The key to producing highly accurate velocity models and images is how the imaging techniques are combined into a workflow that mitigates any weakness that might exist in any one method alone; see Rønholt et al. (2014), and references therein, for a complete description.

Aided by the rich low-frequency data recorded by broadband dual-sensor seismic data, FWI produces high-resolution velocity model updates from the seafloor down to depths where the refracted energy diminishes. Indeed, in the BSSE the velocities show excellent structural shut-off (with low velocity zones conforming precisely to structure). In addition, the broad frequency content ensures that the vertical resolution of velocity models is excellent; see Figure 4 for example.

Towed streamer EM inversion methodology

We use unconstrained inversion of the Towed Streamer EM data to determine the sub-surface resistivity as we aim to maximise the information gained from the EM data without constraining the model. Previous case studies show that the data-density of Towed Streamer EM data enables the reliable and accurate determination of sub-surface resistivity using unconstrained inversion; see for example McKay et al. (2015). In any case, in a frontier exploration setting such as the BSSE then geological knowledge is limited: there are no wells and little a-priori information to provide model parameter constraints. Regardless, we need to ensure that the resistivity model is an independent source of information: We wish to investigate the correlation between the velocity and resistivity, not induce correlation.

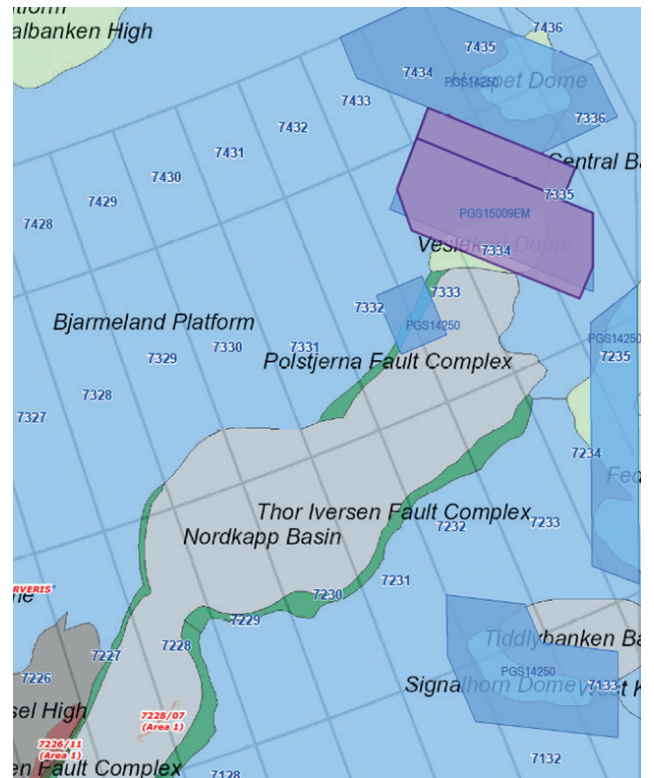
The Towed Streamer EM data were inverted in 3D using the unconstrained anisotropic inversion methodology outlined by Zhdanov et al. (2014). No seismic data and/or resistivity parameter constraints are used to restrict the determination of the vertical and horizontal resistivity, or anisotropy. A key fea-

ture of the 3D inversion is the footprint methodology where the data are inverted all at once, but the modelling domain is decomposed into numerous sub-domains based on sensitivity measures. This decomposition enables large-scale and efficient inversion, and a single consistent model. In general, the inversion model quality is good throughout the study area with a relative data misfit of < 3%.

Joint interpretation

One practical advantage of undertaking the CWI workflow is that both the seismic and EM volumes are in the depth domain. This makes the initial data integration relatively trivial although we do have to be mindful of the differing resolution of the acoustic and electromagnetic properties. Nevertheless, the first step in the workflow is to simply overlay seismic and EM volumes to examine the degree of conformance between, for example, the main stratigraphic boundaries and resistivity units. However, for brevity we do not show an example here.

The second step is to compare the high-resolution velocity and sub-surface resistivity models. To enable comparison of the lateral variations in velocity and resistivity on approximately the same scale, we extracted the average velocity and resistivity over a given depth interval. In Figure 5, the average FWI velocity, unconstrained vertical resistivity and anisotropy, extracted over a 200 m interval below an



EM & Potential Methods

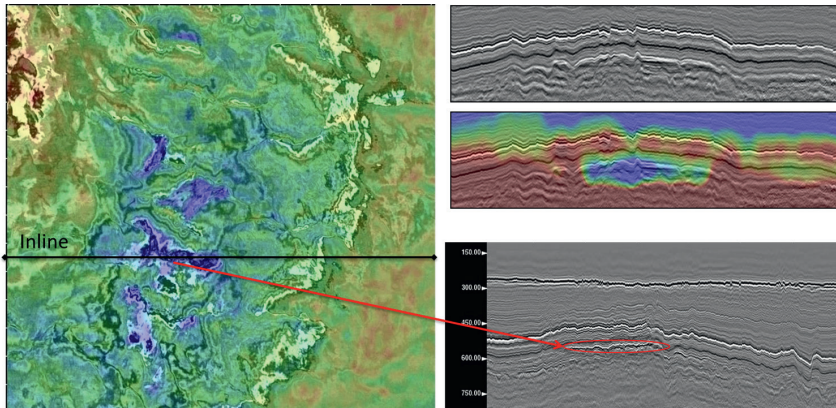


Figure 4 FWI Velocity overlay on Kirchhoff PSDM. The depth slice (left) and corresponding in-line section (lower right) show that the low velocity zones identified from refraction-based inversion correlates well with (amplitude) bright spots seen in the reflection imaging. The in-line section (upper right) highlights the high resolution of the velocity model with frequencies up to 18 Hz delineating the low velocity zones at about 600 m depth.

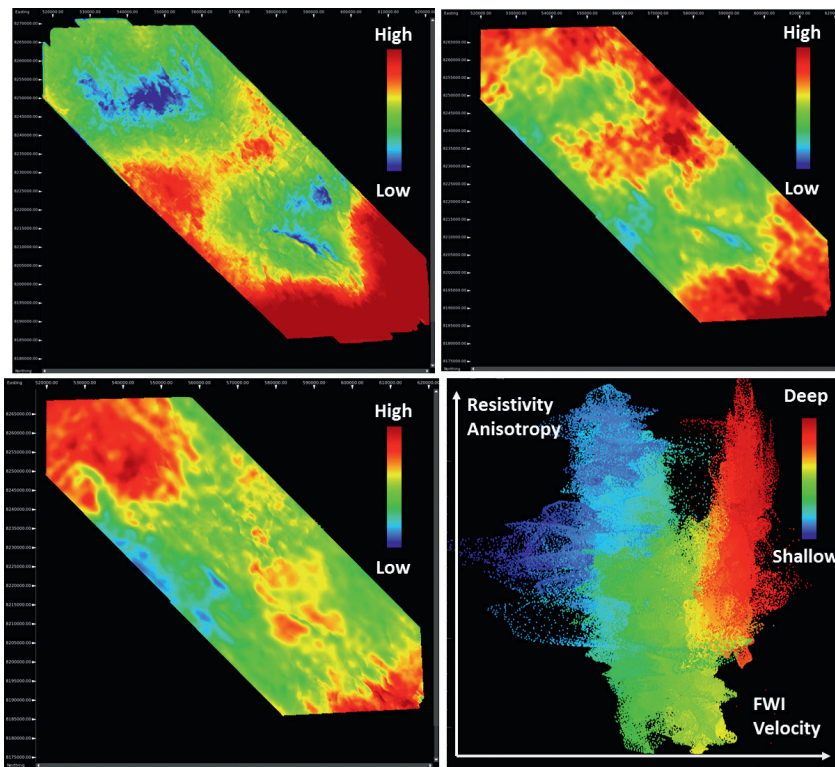


Figure 5 Average attributes extracted over a 200 m interval of interest: FWI Velocity (top left), Vertical Resistivity (top right) and resistivity anisotropy (bottom left). Cross plot of resistivity anisotropy vs. FWI velocity over the same 200 m interval: the colour coding indicates depth and spans a range of about 500 m.

interpreted horizon, are shown. First of all, the FWI velocities show clearly that there are two obvious low-velocity structures: These correspond to the two main structural highs in the area. Closer examination of the FWI velocities reveals that many of the low-velocity features correspond very well with the structural highs and other acoustic features such as potential flat spots and amplitude brightening (see Figure 4 also). Indeed, detailed reservoir characterization analysis indicates that the low-velocity zones correlate extremely well with other attributes such as low acoustic impedance and low V_p/V_s (derived from AVA inversion of pre-stack data from separated wavefield imaging). However, the same depth interval is relatively resistive off-structure and more conductive on-structure, which at first may be disappoint-

ing from the exploration perspective since in general we are expecting high resistivity if the sands within the depth interval are hydrocarbon charged. Nevertheless, the gross lateral trends in resistivity and velocity are comparable (with a positive correlation between resistivity and velocity) which suggests that the same mechanism (e.g. depth trend or change of facies) is driving the variation of both. It is likely that the overall background trend in resistivity may be masking more subtle variations of interest.

The third step is to estimate the background trend in sub-surface resistivity from the unconstrained resistivity, which could be attempted in a number of ways. We chose to determine the average background vertical resistivity over the same depth interval by predicting it from the

horizontal resistivity using an estimate of regional anisotropy ($\rho_v/\rho_h \approx 5$; where ρ_v and ρ_h are the vertical and horizontal resistivity respectively). The predicted background vertical resistivity was then subtracted from the resistivity model to determine an anomalous vertical resistivity. We found that in this case the spatial variation of the anomalous vertical resistivity is very similar to the anisotropy shown in Figure 5 with increases in the anomalous vertical resistivity confined mainly to the structural highs.

As the final step, we examined the relation between the various attributes via cross-plots. In Figure 5, a cross-plot of resistivity anisotropy (ρ_v/ρ_h) and FWI velocity is shown with the colour coding denoting interval depth (blue shallow; red deep). Clearly, there is some degree of correspondence between high anisotropy (and therefore potentially anomalous vertical resistivity), low velocity and the shallowest depths (structural highs).

Summary and conclusions

A high-resolution velocity model is but one of the products of the CWI workflow enabled by broadband dual-sensor seismic data. Combining the high-resolution velocity model with the unconstrained sub-surface resistivity model enables a relatively quick and easy integration of acoustic and electromagnetic rock properties that have complementary sensitivity to lithology and fluid content. The correlation between the variation in velocity and resistivity implies that if we can understand the background trend in at least one of the properties then we may be able to exploit the correlation to define a robust background trend and thus define anomalous areas of interest, e.g. anomalously high resistivity associated with low velocity.

If either rock property were interpreted alone there would be ambiguities that could translate to increased risk of a false-positive scenario from the commercial discovery perspective (e.g. prediction of commercial hydrocarbon volumes when there are only residual hydrocarbons). Thus, with the development of reliable and cost-effective methods to determine the sub-surface velocity and resistivity, based fundamentally on broadband dual-sensor seismic and Towed Streamer EM data, then complementary rock properties can be interpreted jointly even before detailed reservoir/quantitative seismic interpretation studies are undertaken (e.g. as a pre-cursory activity). Doing so has the potential to enable ranking and/or improve de-risking of prospects in a frontier exploration setting e.g. by ensuring that support for a given play and/or prospect is provided by more than one geophysical data-set.

For the brief case-study we considered here, we find a positive correlation (e.g. high velocity = high resistivity) between the spatial variation of the velocity and resistivity for the interval of interest. Indeed, the interval we considered encompasses both shales and potential reservoir sands.

However, when we removed the overall background trend in resistivity we found that areas of increased resistivity tend to correspond to areas of low velocity and structural highs, highlighting the exploration potential of the area and interval we considered.

We presented only unconstrained EM inversion in this study (which produces smooth resistivity models that tend to smear resistivity in depth and across interfaces between different rock types). Obvious next steps are to focus in on the areas of interest to try to determine the origin of the resistivity and velocity anomalies using, for example, a combination of guided EM inversion (e.g. McKay et al., 2015) together with more detailed quantitative interpretation of the seismic data.

Acknowledgments

We would like to thank PGS for permission to publish this work, and to our PGS colleagues for their valuable input and contribution to this study, as well as the seismic and EM imaging and inversion projects. TechnoImaging, LLC performed the 3D EM inversion on our behalf: our thanks go to Masashi Endo and David Sunwall.

References

- Brevik, I., Gabrielsen, P.T. and Morten, J.P. (2009). The role of EM rock physics and seismic data in integrated 3D CSEM data analysis. *79th SEG Meeting*, Expanded Abstracts, 835-839.
- Carcione, J.M., Ursin, B., and Nordskog, J.I. (2007). Cross-property relations between electrical conductivity and the seismic velocity of rocks. *Geophysics*, 72(5), PE193-E204.
- Faust, L.Y. (1953). A velocity function including lithologic variation. *Geophysics*, 18, 271-288.
- MacGregor, L. (2012). Integrating seismic, CSEM, and well-log data for reservoir characterization. *The Leading Edge*, 31(3), 268-277.
- McKay, A., Mattsson, J. and Du, Z. (2015). Towed Streamer EM – reliable recovery of sub-surface resistivity. *First Break*, 33, 75-85.
- Rønholt, G., Korsmo, Ø., Brown, S., Valenciano, A., Whitmore, D., Chemingui, N., Brandsberg-Dahl, S., Dirks, V. and Lie, J. E. (2014). High-fidelity complete wavefield velocity model building and imaging in shallow water environments – A North Sea case study. *First Break*, 32, 127-131.
- Veggeland, T., Vold, B.F., Olstad, R. and Janke, A. (2014). The Wisting oil discovery: using CSEM and seismic attributes. *Hydrocarbon Habitats Seminar*, 3.
- Werthmüller, D., Ziolkowski, A. and Wright, D. (2013). Background resistivity model from seismic velocities. *Geophysics*, 78, E213-E223.
- Werthmüller, D. (2013). Bayesian estimation of resistivities from seismic velocities. PhD Thesis, University of Edinburgh.
- Zhdanov, M.S., Endo, M., Yoon, D., Cuma, M., Mattsson, J. and Midgley, J. (2014). Anisotropic 3D inversion of towed streamer electromagnetic data: Case study from the Troll West Oil Province. *Interpretation*, 2(3), p. SH01-SH17.